ARTICLE   OPEN

Low-cost, μm-thick, tape-free electronic tattoo sensors with minimized motion and sweat artifacts

Youhua Wang [1,2,3], Yitao Qiu[1,7], Shideh Kabiri Ameri[4], Hongwoo Jang[5], Zhaohe Dai[1], YongAn Huang[2,3] and Nanshu Lu [1,4,5,6]

Electronic tattoos (e-tattoos), also known as epidermal electronics, are ultra-thin and ultra-soft noninvasive but skin-conformable devices with capabilities including physiological sensing and transdermal stimulation and therapeutics. The fabrication of e-tattoos out of conventional inorganic electronic materials used to be tedious and expensive. Recently developed cut-and-paste method has significantly simplified the process and lowered the cost. However, existing cut-and-paste method entails a medical tape on which the electronic tattoo sensors should be pasted, which increases tattoo thickness and degrades its breathability. To address this problem, here we report a slightly modified cut-and-paste method to fabricate low-cost, open-mesh e-tattoos with a total thickness of just 1.5 μm. E-tattoos of such thinness can be directly pasted on human skin and conforms to natural skin texture. We demonstrate that this ultra-thin, tape-free e-tattoo can confidently measure electrocardiogram (ECG), skin temperature, and skin hydration. Heart rate and even respiratory rate can be extracted from the ECG signals. A special advantage of such ultra-thin e-tattoo is that it is capable of high-fidelity sensing with minimized motion artifacts under various body movements. Effects of perspiration are found to be insignificant due to the breathability of such e-tattoos.

INTRODUCTION

Noninvasive wearable devices mounted on skin, the largest organ of human body, provide a versatile means to acquire information about the body or to deliver stimulation and drugs to the body. They are believed to have the potential to revolutionize mobile health, assistive technology, athletic training, human machine interaction, and many other fields. Currently, a key challenge to wearable devices is the mechanical mismatch between the soft, curvilinear, and dynamic skin and the rigid, planar, and fragile wafer-based electronics and sensors. Most state-of-the-art commercial wearables are using straps or tapes to fix rigid device boxes on the body. The insecure skin–sensor interface makes these devices suffer from limited functionality and signal-to-noise ratio, as well as significant motion artifacts.

With the development of intrinsically soft electronic materials,[1,2] flexible and stretchable structures,[3,4] and novel material processing techniques,[5,6] flexible and stretchable electronics become feasible. In addition to well-known applications such as flexible display[7] and e-skin,[8] flexible and stretchable electronics also become a viable solution for bio-integrated electronics,[9] which have found exploding use in physiological signal and sweat monitoring,[10–16] external signal sensing[17,18] and information displaying.[18,19] Among many breakthroughs, epidermal electronics,[10] also known as electronic tattoos (e-tattoos), emerge as a class of promising candidates for wearable electronics. E-tattoos are ultra-thin and ultra-soft electronics, sensors, and actuators, whose stiffness and mass density match well with those of human epidermis.[10,11,17] Because of such distinct mechanical properties,

e-tattoos are able to achieve ultimate conformability to various skin textures, forming noninvasive but the most intimate coupling with skin.[20–25] The softness and conformability offer several unique advantages over conventional thick and stiff sensors. First, conformable contact enlarges the contact area between the sensors and the skin, which can effectively lower the contact impedance and facilitate signal transfer across the sensor–skin interface. Second, when skin deforms, e-tattoos would be able to follow skin displacement, minimizing interfacial slippage and as a result, motion artifacts.[26] Ultra-thin and ultra-lightweight imperceptible plastic electronics have also been reported.[27,28] But they are not stretchable, hence would still be susceptible to sliding against skin under significant deformation.

Nevertheless, the thinness and softness of e-tattoos greatly limit their reusability. Therefore lowering their cost has practical significance. The main steps of the current fabrication method of e-tattoos can be summarized as patterning by photolithography[10,29–31] and transfer printing,[6,32,33] which are expensive, time consuming, and incompatible with roll-to-roll process.[34] As a remedy for the costly fabrication process, we have invented a dry and freeform desktop fabrication method for e-tattoos called the cut-and-paste method.[34] In this method, sensors and circuits are cut out of commercially available metalized polymer sheets using a benchtop programmable mechanical cutter plotter. There is no need of any chemical or cleanroom facilities and the overall processing time can be reduced to minutes. However, the thickness of commercially available metalized polymer sheets we could find is at least 13 μm, which limits their conformability to

---

[1]Center for Mechanics of Solids, Structures and Materials, Department of Aerospace Engineering and Engineering Mechanics, The University of Texas at Austin, Austin, TX 78712, USA; [2]State Key Laboratory of Digital Manufacturing Equipment and Technology, Huazhong University of Science and Technology, Wuhan, China; [3]Flexible Electronics Research Center, Huazhong University of Science and Technology, Wuhan, China; [4]Deparment of Electrical and Computer Engineering, The University of Texas at Austin, Austin, TX, USA; [5]Texas Materials Institute, The University of Texas at Austin, Austin, TX, USA and [6]Department of Biomedical Engineering, The University of Texas at Austin, Austin, TX, USA
Correspondence: YongAn Huang (yahuang@hust.edu.cn) or Nanshu Lu (nanshulu@utexas.edu)
[7]Present address: Department of Civil & Environmental Engineering, Stanford University, Stanford, CA 94305, USA

npj

Low-cost, µm-thick, tape-free electronic tattoo
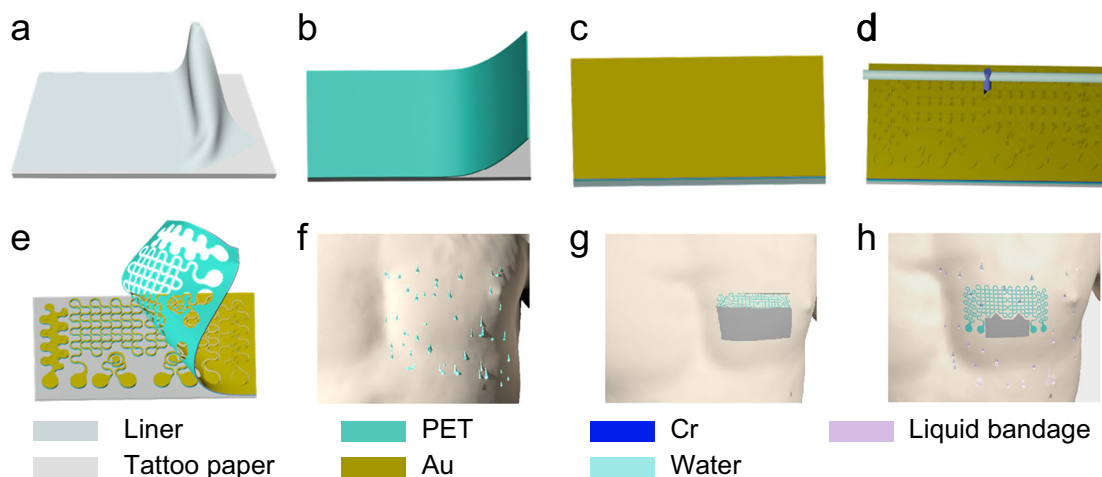Y Wang et al.

2

Fig. 1   Schematics of the cut-and-paste manufacturing processes for ultra-thin, tape-free e-tattoo. **a** Removing the liner from commercial tattoo paper. **b** Laminating 1.4-µm-thick transparent PET sheet on the tattoo paper. **c** Depositing 10-nm-thick Cr and 100-nm-thick Au on the PET with thermal evaporator. **d** Patterning the Au/Cr/PET sheet with a commercial cutter plotter. **e** Peeling off the extraneous parts from the tattoo paper. **f** Applying little water on human skin. **g** Pasting e-tattoo on human skin from tattoo paper. **h** Spraying liquid bandage over the e-tattoo with the hydration sensors being covered by a stencil

skin. To hold sheets of such thickness for mechanical cutting, strong enough but releasable adhesives such as thermal release tape has to be employed as the supporting substrate. To secure sensors of such thickness on skin, the sensors are first transferred on an adhesive tape such as the 3 M Tegaderm tape and this tape together with the sensors is patched on the skin. Although stretchable and transparent, Tegaderm has a thickness of 47 µm and Young's modulus of 7.4 MPa,[34] which somewhat blocks skin breathing and mechanically constrains the skin. In fact, using conventional microfabrication and transfer printing method, tape-free e-tattoos with a total thickness of only 0.8 µm can be directly printed on the skin.[20] Tape-free e-tattoos made out of 65-nm-thick gold nanomeshes patterned by shadow masks have also been reported very recently.[14] Therefore, how to apply the freeform cut-and-paste method to create a low-cost, µm-thick, and more importantly, tape-free e-tattoo is the focus of this paper.

In this paper, we report a cut-and-pasted e-tattoo that is only 1.5 µm thick and can be directly pasted on human skin like a temporary transfer tattoo. This e-tattoo is tape-free and designed into an open-mesh filamentary structure, which makes it breathable and exhibit negligible stiffness.[35] It includes multiple sensors and can synchronously measure skin temperature, skin hydration, and electrocardiogram (ECG). Heart rate and respiratory rate can be extracted from the ECG signals. Attributing to its ultimate softness and conformability, we will demonstrate that ECG measured by this µm-thick e-tattoo suffers from reduced motion artifacts compared with thicker e-tattoos and even gel electrodes. Because of its open-mesh design, sweat does not accumulate between e-tattoo and skin, which helps minimize sweat artifacts.

RESULTS AND DISCUSSION

Schematics in Fig. 1 illustrate the cut-and-paste fabrication process of our open-mesh e-tattoo. It begins with peeling off the liner of a slightly wetted commercial tattoo paper (Silhouette, USA) (Fig. 1a and Fig. S1a) and laminating a 1.4-µm-thick transparent PET (polyethylene terephthalate) sheet (PolyK Technologies, LLC, USA) on the tattoo paper (Fig. 1b and Fig. S1b), followed by drying on a hotplate at 50–60 °C for ~5 min. The pre-existing water-soluble adhesive on the tattoo paper can securely hold the thin PET sheet during the whole fabrication process, even after high temperature treatment (100–160 °C, shown in Fig. S2), and will be dissolved when the e-tattoo is ready to be pasted on skin. Next, 10-nm-thick

chromium (Cr) and 100-nm-thick gold (Au) were deposited on the PET (Fig. 1c and Fig. S1c) using a thermal evaporator. Thin film Au is chosen as the electrode and resistance temperature detector (RTD) material for its biocompatibility, chemical inertness, as well as ductility. A cheaper alternative is titanium (Ti) but it is not as ductile as Au. The Au/Cr/PET film was cut by a programmable mechanical cutter plotter (Silhouette Cameo, USA) to form serpentine-shaped seams according to an AutoCAD design imported into the Silhouette Studio® software (Fig. 1d and Fig. S1d). In the software, the sharpness was set to be 5, the cutting rate 2, and the thickness 1. Slightly wetting the tattoo paper can partially dissolve the pre-existing water-soluble adhesive (Fig. S1e), such that the extraneous parts of the Au/Cr/PET can be easily peeled off from the tattoo paper, leaving filamentary-serpentine-shaped stretchable sensors (Fig. 1e, Fig. S1f and Supplementary Video 1). In addition to Au/PET, we have demonstrated that the cutter plotter can also be used to pattern Al/PET,[36] carbon-doped thin film PDMS,[36] graphene/PMMA,[24] and even indium tin oxide (ITO) on PET.[36] After the peeling, tattoo papers were dried on a hotplate at 50–60 °C for ~5 min again. Thirteen-micrometer-thick Au/PET strips were cut out of commercially available Au/PET sheets (Rotex Tech, llc.) and used as intermediate connectors to conduct signals captured by the e-tattoo. One end of the Au/PET strip was attached to a terminal of the e-tattoo via silver (Ag) paste (124-23, Creative Materials, USA) and the other end can be alligator clipped. As there are eight terminals on the e-tattoo, eight Au/PET strips were attached on by one. To paste the e-tattoos directly on human skin, we first moisturized our skin with water to increase the capillary force (Fig. 1f) and then laminated the tattoo paper on the skin. Note that we did not scrub the skin to remove stratum corneum prior to mounting the e-tattoo. After fully wetting the tattoo paper, slowly sliding the tattoo paper off the e-tattoo can yield a successful transfer to human skin (Fig. 1g and Fig. S1g). We found that sliding was more effective than peeling probably because the partially dissolved water-soluble adhesive is very slippery but still tacky in some areas. After the transfer, a 1.5-µm-thick tape-free and open-mesh e-tattoo can adhere on the skin purely via van der Waals (vdW) forces. To offer some protection to the open-mesh e-tattoo, we sprayed breathable liquid bandage (3 M Nexcare, USA) over the e-tattoo with the hydration sensors covered by a paper stencil (Fig. 1h and Fig. S1h). Each spray yields ~200-nm-thick transparent solid polymer coating after solidification so we normally spray five

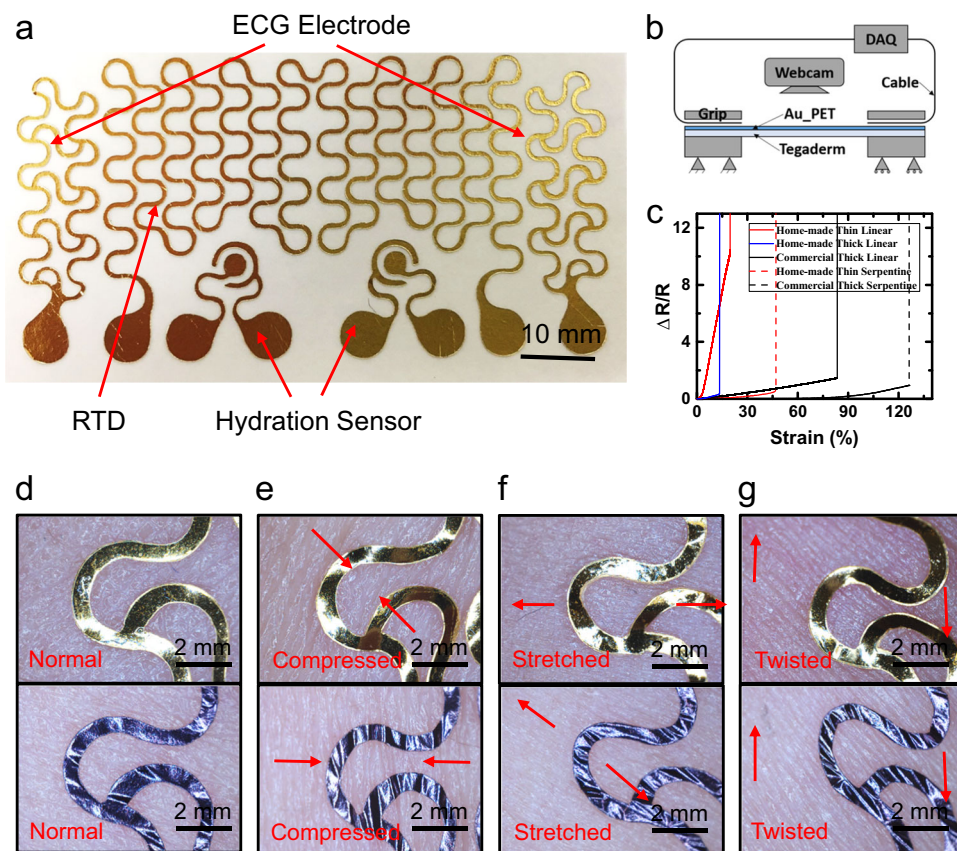Low-cost, µm-thick, tape-free electronic tattoo
Y Wang et al.

npj

3

Fig. 2 Mechanical characterizations of e-tattoo. **a** Top view of an e-tattoo incorporating two ECG electrodes, two hydration sensors, and an RTD, all in filamentary serpentine (FS) layout. **b** Schematics of the tensile testing system with *in* situ electrical resistance measurement. **c** Resistance change measured as a function of applied strain. **d**–**g** Conformability of open-mesh 13-µm-thick (upper row) and 1.5-µm-thick e-tattoo on human skin

times to create a transparent encapsulation layer of ~1 µm thick over the e-tattoos. We prefer not to have encapsulations over the hydration sensors because it will slow down lotion absorption in the calibration step. Supplementary Video 2 illustrates the complete skin-transfer process. Although the skin-transfer process is very similar to the transfer of a temporary tattoo, more care is required to transfer e-tattoo because the e-tattoo is an open mesh instead of a continuous film.

Figure 2a is the photograph of an as-fabricated e-tattoo, which houses two ECG electrodes, one RTD, and two hydration sensors. The ribbon width of all filamentary serpentines is 600 µm, as limited by the patterning resolution of the cutter plotter (Fig. S3). Considering the tradeoff between stretchability and overall e-tattoo size, the filamentary serpentine was designed to have a ribbon-width-to-arc-radius ratio of 0.4 and an arc angle of 15°, guided by the mechanics theory of serpentine ribbons.[35] As ECG amplitude has a strong positive correlation with the in-plane distance between the two electrodes,[37] we chose to place the two electrodes 65 mm apart on our e-tattoo. The overall size of this multifunctional e-tattoo is about 7.5 cm × 4.0 cm, which is smaller than a standard credit card (8.56 cm × 5.40 cm).

According to analytical solutions to freestanding serpentines,[35] the tensile stiffness of our open-mesh serpentine ribbon is estimated to be 115 N/m, which is well comparable to the tensile stiffness of human epidermis (160 N/m assuming a uniform material of 160-kPa modulus and 1-mm thickness). The stretchability of those ultra-thin serpentine ribbons was tested by adhering them to a Tegaderm tape. The tensile experiment was performed with in situ electrical resistance measurement using a digital multimeter and webcam observation (Fig. 2b) as the

change in resistance can rigorously reflect the mechanical integrity of the metal ribbon.[38] Figure 2c plots the measured resistance change as a function of the applied tensile strain for several linear (solid curves) and serpentine (dashed curves) ribbons of different thicknesses. We determine stretchability by identifying the first sharp kink in these curves. The black curves are for 13-µm-thick Au/PET ribbons cut out of the commercial Au/PET sheets. Even a linear ribbon can be stretched more than 80% (black solid curve), which suggests that the PET in the commercial Au/PET bilayer sheet is quite stretchable. Regarding the Au film in the commercial bilayer, it must be highly plastically deformable and must have strong adhesion with the PET layer according to a previous study on highly stretchable metal on polymer.[38] After patterning into a serpentine ribbon, its stretchability goes beyond 120% (black dashed curve). Due to their robustness even in linear shape, we chose to use commercial Au/PET to prepare intermediate connectors and thick e-tattoos for comparison later. In contrast, the stretchability of homemade linear Au ribbon is far less, either on 1.4-µm-thick (red solid curve, rupturing at 3.2%) or 13-µm-thick (blue solid curve, rupturing at 14%) PET sheets, which could be attributed to less stretchable PET or less favorable Au film microstructure or Au–PET adhesion. After pattering the ultra-thin Au/Cr/PET to serpentine shape, its stretchability can increase from 3.2 to 45% (red dashed curve), which is beyond skin stretchability (30%).[39] The optical images of a 1.5-µm-thick Au/PET serpentine ribbon before and after being stretched by 35% are provided in Fig. S4. It is evident that the ribbon is still intact after stretch, which agrees with the resistance measurement. To understand the effect of PET thickness on serpentine deformation, we have performed finite element modeling (FEM) for Tegaderm-
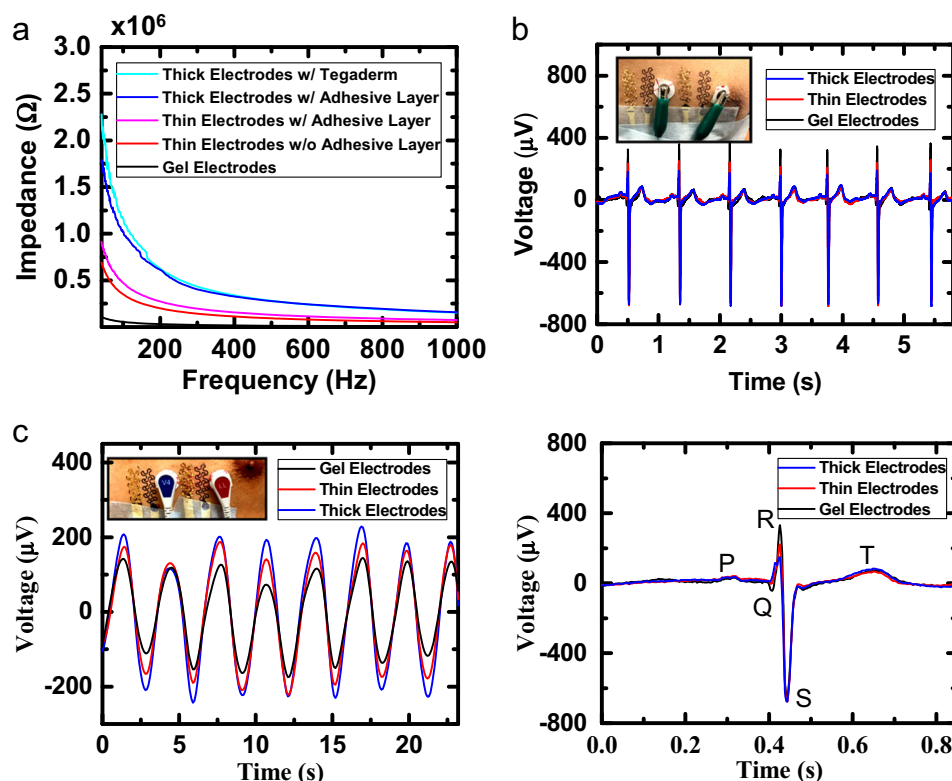
npj

Low-cost, µm-thick, tape-free electronic tattoo
Y Wang et al.

4

Fig. 3 Characterization of ECG tattoo sensor. **a** Skin-electrode interface impedance measured for 13-µm-thick e-tattoo with Tegaderm tape (cyan) and skin adhesive (blue), 1.5-µm-thick e-tattoo with (magenta) and without (red) skin adhesive, and gel electrodes (black). **b** Upper panel: ECG signals synchronously captured by 13-µm-thick e-tattoo (blue), 1.5-µm-thick e-tattoo (red), and gel electrodes (black). Lower panel: zoomed-in ECG signal with characteristic peaks labeled. **c** Respiration rate captured by 13-µm-thick e-tattoo (blue), 1.5-µm-thick e-tattoo (red), and gel electrodes (black)

supported serpentines using ABAQUS. The reason we include a substrate in FEM is because our freestanding FS e-tattoo eventually attaches to the skin, which serves as a substrate. Figure S5a and b display the strain distribution in 1.5-µm-thick and 13-µm-thick serpentines under the same tensile strain (20%) applied to the Tegaderm substrate. It is evident that the thinner serpentine exhibit larger maximum strain at the inner crest. It is because substrate limits serpentine rigid body rotation and hence enlarges maximum strains in serpentine. The thicker the serpentine, the higher stiffness and hence the less substrate constraint. Cyclic test of the 1.5-µm-thick Au/PET serpentine on Tegaderm was performed using a dynamic mechanical analyzer under 20% maximum tensile strain at the frequency of 2 Hz. Resistance change with number of cycles is plotted in Fig. S6. It is found that resistance change is continuous before 1000 cycles. After that, significant jumps can be detected. Therefore, we consider our ultra-thin serpentines to be cyclable up to 1000 times.

In addition to the 1.5-µm-thick e-tattoo shown in Fig. 2a, we also fabricated open-mesh filamentary serpentine ECG electrodes out of the 13-µm-thick commercial Au/PET sheet as a counterpart for performance comparison. To keep the thicker e-tattoo laminated on human skin, a layer of liquid skin adhesive (Tuf-Skin, Cramer, USA) with the thickness of 3–4 µm had to be added between the electrodes and the skin. Figure 2d–g display a series of micrographs comparing the skin-electrode coupling for the thick (upper row) and ultra-thin (lower row) e-tattoos. It is evident that under about 20% compression, stretching, and twisting, the ultra-thin e-tattoos are able to closely follow skin wrinkles while the thick e-tattoos always remain flat. The minimized sliding between the ultra-thin e-tattoo and the skin is believed to be

responsible for the reduced motion artifacts, which will be discussed in detail later.

As skin–electrode interface impedance is directly related to their quality of contact, we measured and compared the impedance for thick electrodes, ultra-thin electrodes, and gel electrodes mounted on human arm using an LCR meter (Rigol), as shown in Fig. 3a. As wet electrodes, silver/silver chloride (Ag/AgCl) gel electrodes (black curve) demonstrate the lowest interface impedance. What is more interesting is to compare the impedance between thick and thin dry electrodes based on filamentary serpentine Au. It can be concluded in Fig. 3a that thick electrodes (blue and cyan curves) have higher impedance than the ultra-thin ones (red and magenta). For ultra-thin electrodes, adding adhesive layer (Tuf-Skin, Cramer, USA) between electrode and skin would lead to slight increase in interface impedance (from red to magenta curves). For thick electrodes, interface impedance is not very sensitive to affixing methods, such as adding adhesive layer between skin and electrode (blue) or adding Tegaderm over the electrode (cyan). Such impedance difference is fully reflected to the ECG signals. As shown in the inset of Fig. 3b upper panel, a pair of open-mesh ultra-thin electrodes w/o any adhesive layer, a pair of open-mesh thick electrodes with adhesive layer, and a pair of trimmed gel electrodes were attached close to the left nipple of a human subject. Forty millimeter distance was ensured between the electrodes in each pair for bipolar ECG measurement. Three-channel ECG was synchronously recorded using a portable wireless multichannel electrical potential recorder (AvatarEEG) with a sampling rate of 1 kHz. After downloading the raw data from AvatarEEG memory, we applied a digital notch filter of 60 Hz and a high pass filter with cut-off frequency of 5 Hz to all data. Three ECG signals plotted in Fig. 3b upper and lower panels indicate that all three types of electrodes can measure identical
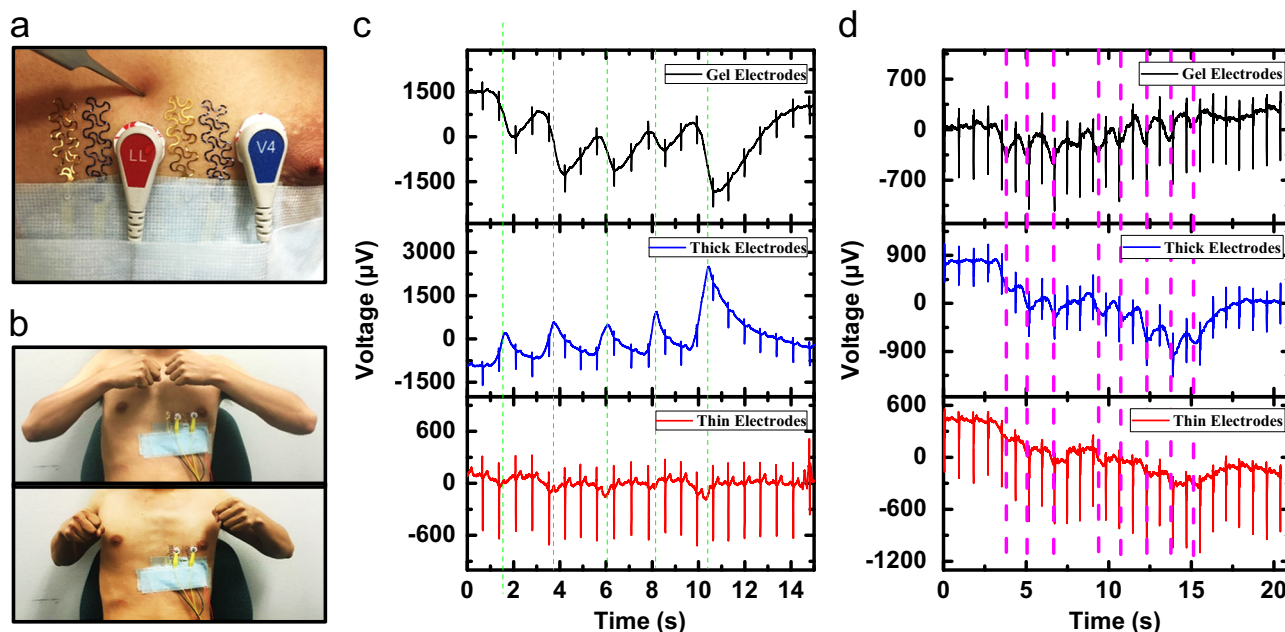
Low-cost, μm-thick, tape-free electronic tattoo
Y Wang et al.

npj

5

Fig. 4 Investigation of motion artifacts. **a** Photograph of human chest being poked by tweezer. **b** Photograph of chest expansion movement. **c** Synchronously measured ECG under motion demonstrated in (**a**). **d** Synchronously measured ECG under motion demonstrated in (**b**). Vertical dashed lines indicate the moments of motion

waves, labeled as the P, Q, R, S, T peaks. The gel electrodes, with the lowest interface impedance, yield the highest signal amplitude (black), followed by the ultra-thin electrodes (red). The thick electrodes have the highest interface impedance, as a result, its signal amplitude is the lowest (blue). If we shift all six electrodes about 4 cm lower than their position in Fig. 3b inset, as shown in Fig. 3c inset, we may also capture the respiration by tracking the position of the S waves, as plotted in Fig. S7 and Fig. 3c. The fluctuation of ECG with respiration can be explained by respiration induced heart-electrode impedance change. During inspiration, lung expansion increases the distance between the heart and the skin and the electrical impedance between the heart and the skin-mounted surface electrodes increases correspondingly, vice versa.[40] While normal respiration leads to periodic fluctuation of the S peak of ECG (Fig. S7a), suffocation after inhalation yields a stable and low amplitude of the S wave (Fig. S7b) because of the constant and large heart-electrode impedance. In contrast, suffocation after exhalation leads to a stable and high amplitude of the S wave (Fig. S7c). Comparing the three different types of electrodes, Fig. 3c suggests that electrodes with larger skin-electrode impedance measures higher fluctuation in S wave due to respiration.

Except for respiration, skin motion and body movements would also result in heart-electrode impedance change and even mechanical slippage between skin and electrodes, both of which contribute to the so-called motion artifacts. To investigate the effects of motion on the ultra-thin e-tattoo, we carried out ECG measurements under different modes of motion, including skin indentation and chest expansion, as illustrated by Fig. 4a, b. Thick electrodes with interface adhesives and gel electrodes were also applied for comparison. ECG measured under skin indentation is offered in Fig. 4c and Supplementary Video 3 and under chest expansion in Fig. 4d and Supplementary Video 4. Vertical dashed lines in Fig. 4c, d indicate the moments of motion applied, and corresponding pits can be clearly observed in the ECG signals measured by gel and thick electrodes. Under both modes of motions, we can conclude that the ultra-thin electrodes (red) suffer from least motion artifacts compared with gel electrodes (black) and thick electrodes (green). Similar to respiration-induced

fluctuation, we can use high skin-electrode impedance to explain the observation that thick electrodes are more sensitive to motion artifacts than ultra-thin tattoo electrodes. However, the sensitivity to motion of gel electrodes is unexpected because they have the lowest skin-electrode impedance. There are two possible sources of motion artifacts in gel electrodes: first, the adhesive annuli of the commercial gel electrodes were trimmed to shrink their footprints, which may degrade skin–electrode coupling during motion; second, the gel electrodes were connected to external cables through a snap button, which may be sensitive to motion. In any case, the motion artifacts in gel electrodes can be observed in both videos and we proved that our ultra-thin electrodes were able to demonstrate superior stability under localized skin motion. Ideally, more vigorous activities such as running or jumping should be tested. But as we still used wires for data acquisition, the motion artifacts associated with swaying wires would be too significant to illustrate the stability of the e-tattoo.

Unlike the motion artifacts, sweat artifacts of e-tattoos have not been reported before. We designed an experiment to induce perspiration, and synchronously measure skin temperature, skin hydration, ECG, and heart rate using one integrated e-tattoo as shown in Fig. 5a. Skin temperature was measured using the RTD and skin hydration was measured by the dot-ring hydration sensor, both of which have been reported for cut-and-pasted 13-μm-thick e-tattoos before.[34] Details for the calibration and validation of our cut-and-pasted ultra-thin RTD and hydration sensor can be found in the Supplementary Information. After installing the ultra-thin e-tattoos on the subject, we simultaneously started skin temperature, skin hydration, and ECG measurements. The results are displayed in Fig. 5b–e. Heart rate was obtained by counting the number of R waves for a moving window of 60 s in ECG. Figure 5f plots magnified views of ECG which are selected from three different periods in Fig. 5e. At $t = 0$ s, the initial skin temperature was measured to be 31.4 °C, skin hydration 65, heart rate 59. Initial ECG was stable and uniform. At $t = 300$ s (Line I), we turned on a 40 W heating fan (H-5210, OPTIMUS) to blow hot wind towards the subject from a distance about 40 cm. In the meanwhile, the subject was asked to start drinking warm water and consuming high-calorie food (fried
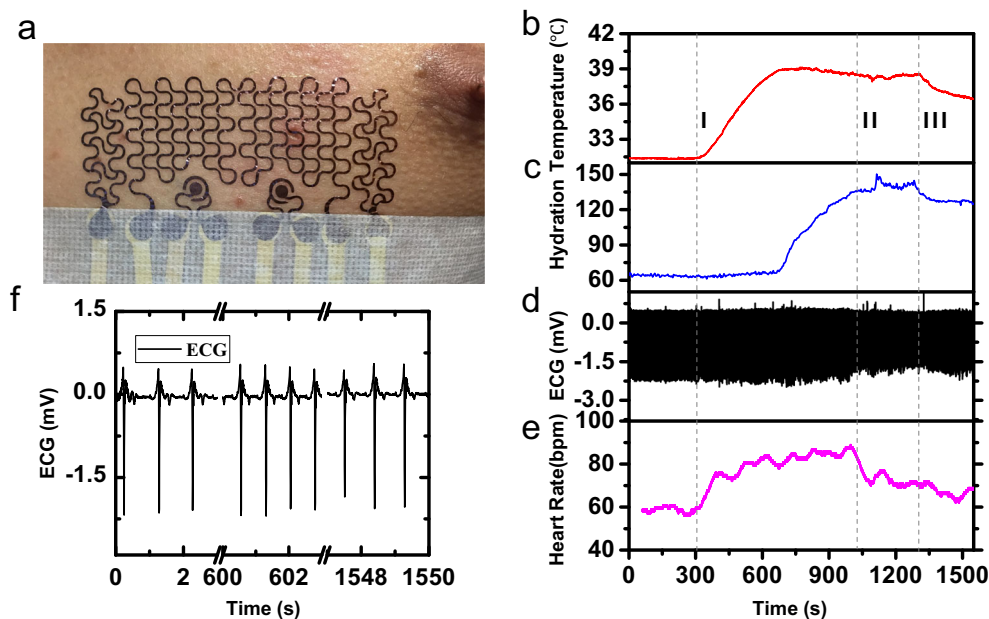
npj

Low-cost, μm-thick, tape-free electronic tattoo
Y Wang et al.

6

Fig. 5 Investigation of sweat artifacts. **a** A 1.5-μm-thick multifunctional e-tattoo transferred on human chest and connected to data acquisition systems. **b**–**e** Skin temperature, skin hydration, ECG, and heart rate simultaneously captured by the e-tattoo before, during, and after the subject was subjected to heating and calorie intake. **f** Zoomed-in ECG signals at different time segments

chicken). We found that skin temperature and heart rate immediately responded to the heating, which has also been observed in other studies.[41] But skin hydration did not start to increase until $t = 667$ s, which is recognized as the beginning of perspiration. As soon as the subject started to sweat, the skin temperature and heart rate stopped rising, which is a demonstration of the powerful thermoregulation system of our body. After $t = 667$ s, skin hydration kept increasing as sweat filled up the sweat glands with a decreasing slope and skin temperature slowly decreased and heart rate sustained. Skin hydration tended to saturate at values around 136 starting from $t = 1029$ s, which indicates that sweat finally reached the surface of skin. At $t = 1029$ s (Line II), the subject was asked to stop drinking and eating but we kept the heating fan on. It is observed that skin temperature and skin hydration try to stay constant with slight fluctuation, which suggests that cyclic sweating and drying of the skin is trying to maintain an new equilibrium between heat production and heat loss.[42] It is also obvious that heart rate dropped to a new constant immediately after the calorie intake stopped. At $t = 1305$ s (Line III), we stopped the heating fan. As a result, skin temperature, skin hydration, and heart rate all started to decrease. The immediate drop in skin temperature, skin hydration, and heart rate indicates very effective sweat evaporation and heat dissipation, which is the result of our open-mesh tape-free e-tattoo. During the whole experiment, ECG has been successfully captured without any noticeable artifacts (Fig. 5d, f).

CONCLUSION

Through an improved dry and freeform cut-and-paste method, we have fabricated a low-cost, 1.5-μm-thick, tape-free, and multifunctional e-tattoo. This e-tattoo can adhere to human skin like a temporary transfer tattoo via just van der Waals forces and it forms an open-mesh filamentary serpentine network on the skin, which allows for superior compliance and breathability. Such ultrathin e-tattoo has demonstrated clear advantages over relatively thick e-tattoos (13-μm thick) in terms of skin–electrode interface impedance, motion artifacts, and sweat artifacts. It has been successfully applied to synchronously measure skin temperature, skin hydration, ECG, and heart rate during perspiration and no

signal degradation was detected. Such low-cost, tape-free, and high-performance e-tattoos represent another meaningful progress towards disposable wearables.

METHODS

All experiments were conducted under approval from the Institutional Review Board at the University of Texas at Austin (protocol number: 2015-05-0024). More details can be seen the Supplementary Information.

Data Availability

All data generated or analyzed during this study are included in this published article (and its Supplementary Information Files) or are available from the corresponding author upon request. The computer code generated during the current study is available from the corresponding author on request.

AUTHOR CONTRIBUTIONS

Processes and experiments were designed by Y.W. and N.L. and performed by Y.W., Y. Q., S.K.A., and H.J. FEM was performed by Y.Q., N.L. supervised the overall research. Y. W., S.K.A., Z.D., Y.A.H., and N.L. contributed to the writing of the manuscript.

ADDITIONAL INFORMATION

Supplementary information accompanies the paper on the *npj Flexible Electronics* website (https://doi.org/10.1038/s41528-017-0019-4).

Competing interests: The authors declare no competing financial interests.

Publisher's note: Springer Nature remains neutral with regard to jurisdictional claims in published maps and institutional affiliations.

Low-cost, μm-thick, tape-free electronic tattoo
Y Wang et al.

7

REFERENCES

1. Forrest, S. R. The path to ubiquitous and low-cost organic electronic appliances on plastic. *Nature* **428**, 911–918 (2004).
2. Oh, J. Y. et al. Intrinsically stretchable and healable semiconducting polymer for organic transistors. *Nature* **539**, 411–415 (2016).
3. Lu, N. & Yang, S. Mechanics for stretchable sensors. *Curr. Opin. Solid State Mater. Sci.* **19**, 149–159 (2015).
4. Rogers, J. A., Someya, T. & Huang, Y. Materials and mechanics for stretchable electronics. *Science* **327**, 1603–1607 (2010).
5. Fukuda, K. & Someya, T. Recent progress in the development of printed thin-film transistors and circuits with high-resolution printing technology. *Adv. Mater.* **29**, 1602736 (2017).
6. Carlson, A., Bowen, A. M., Huang, Y., Nuzzo, R. G. & Rogers, J. A. Transfer printing techniques for materials assembly and micro/nanodevice fabrication. *Adv. Mater.* **24**, 5284–5318 (2012).
7. Lee, S.-M., Kwon, J. H., Kwon, S. & Choi, K. C. A review of flexible OLEDs toward highly durable unusual displays. *IEEE Trans. Electron Dev.* **64**, 1922–1931 (2017).
8. Hammock, M. L., Chortos, A., Tee, B. C. K., Tok, J. B. H. & Bao, Z. 25th anniversary article: the evolution of electronic skin (e-skin): a brief history, design considerations, and recent progress. *Adv. Mater.* **25**, 5997–6038 (2013).
9. Kim, D. H., Ghaffari, R., Lu, N. S. & Rogers, J. A. Flexible and stretchable electronics for bio-integrated devices. *Annu. Rev. Biomed. Eng.* **14**, 113–128 (2012).
10. Kim, D.-H. et al. Epidermal electronics. *Science* **333**, 838–843 (2011).
11. Yeo, W. H. et al. Multifunctional epidermal electronics printed directly onto the skin. *Adv. Mater.* **25**, 2773–2778 (2013).
12. Lee, H. et al. A graphene-based electrochemical device with thermoresponsive microneedles for diabetes monitoring and therapy. *Nat. Nano* **11**, 566–572 (2016).
13. Lee, H. et al. Wearable/disposable sweat-based glucose monitoring device with multistage transdermal drug delivery module. *Sci. Adv.* **3**, e1601314 (2017).
14. Miyamoto, A. et al. Inflammation-free, gas-permeable, lightweight, stretchable on-skin electronics with nanomeshes AOP. *Inflammation* **1**, 17 (2017).
15. Bandodkar, A. J., Jia, W. & Wang, J. Tattoo-based wearable electrochemical devices: a review. *Electroanalysis* **27**, 562–572 (2015).
16. Gao, W. et al. Fully integrated wearable sensor arrays for multiplexed in situ perspiration analysis. *Nature* **529**, 509–514 (2016).
17. Kim, J. et al. Epidermal electronics with advanced capabilities in near-field communication. *Small* **11**, 906–912 (2015).
18. Song, J.-K. et al. Wearable force touch sensor array using a flexible and transparent electrode. *Adv. Funct. Mater.* **27**, 9 (2017).
19. Yokota, T. et al. Ultraflexible organic photonic skin. *Sci. Adv.* **2**, e1501856 (2016).
20. Yeo, W. H. et al. Multi-functional electronics: multifunctional epidermal electronics printed directly onto the skin. *Adv. Mater.* **25**, 2772–2772 (2013).
21. Jeong, J. W. et al. Materials and optimized designs for human-machine interfaces via epidermal electronics. *Adv. Mater.* **25**, 6839–6846 (2013).
22. Wang, S. et al. Mechanics of epidermal electronics. *J. Appl. Mech.* **79**, 031022 (2012).
23. Wang, L. & Lu, N. Conformability of a thin elastic membrane laminated on a soft substrate with slightly wavy surface. *J. Appl. Mech.* **83**, 041007 (2016).
24. Kabiri Ameri, S. et al. Graphene electronic tattoo sensors. *ACS Nano* **11**, 7634–7641 (2017).
25. Wang, L., Qiao, S., Kabiri Ameri, S., Jeong, H. & Lu, N. A thin elastic membrane conformed to a soft and rough substrate subjected to stretching/compression. *J. Appl. Mech.* **84**, 111003–111009 (2017).
26. Jeong, J. W. et al. Capacitive epidermal electronics for electrically safe, long-term electrophysiological measurements. *Adv. Healthc. Mater.* **3**, 642–648 (2014).
27. Kaltenbrunner, M. et al. An ultra-lightweight design for imperceptible plastic electronics. *Nature* **499**, 458 (2013).
28. Melzer, M. et al. Imperceptible magnetoelectronics. *Nat. Commun.* **6**, 6080 (2015).
29. Lu, N. & Kim, D.-H. Flexible and stretchable electronics paving the way for soft robotics. *Soft Robot.* **1**, 53–62 (2014).
30. Dagdeviren, C. et al. Conformable amplified lead zirconate titanate sensors with enhanced piezoelectric response for cutaneous pressure monitoring. *Nat. Commun.* **5**, 4496 (2014).
31. Meitl, M. A. et al. Transfer printing by kinetic control of adhesion to an elastomeric stamp. *Nat. Mater.* **5**, 33–38 (2006).
32. Kim, S. et al. Microstructured elastomeric surfaces with reversible adhesion and examples of their use in deterministic assembly by transfer printing. *Proc. Natl Acad. Sci.* **107**, 17095–17100 (2010).
33. Saeidpourazar, R. et al. Laser-driven micro transfer placement of prefabricated microstructures. *J. Microelectromech. Syst.* **21**, 1049–1058 (2012).
34. Yang, S. et al. "Cut-and-Paste" manufacture of multiparametric epidermal sensor systems. *Adv. Mater.* **27**, 6423–6430 (2015).
35. Widlund, T., Yang, S., Hsu, Y.-Y. & Lu, N. Stretchability and compliance of freestanding serpentine-shaped ribbons. *Int. J. Solids Struct.* **51**, 4026–4037 (2014).
36. Fang, Y., Liu, H., Li, G. & Zhu, X. A multichannel surface EMG system for hand motion recognition. *Int. J. Hum. Robot.* **12**, 1550011 (2015).
37. Nedios, S., Romero, I., Gerds-Li, J.-H., Fleck, E. & Kriatselis, C. Precordial electrode placement for optimal ECG monitoring: implications for ambulatory monitor devices and event recorders. *J. Electrocardiol.* **47**, 669–676 (2014).
38. Lu, N., Wang, X., Suo, Z. & Vlassak, J. Metal films on polymer substrates stretched beyond 50%. *Appl. Phys. Lett.* **91**, 221909 (2007).
39. Silver, F. H., Siperko, L. M. & Seehra, G. P. Mechanobiology of force transduction in dermal tissue. *Skin. Res. Technol.* **9**, 3–23 (2003).
40. Travaglini, A., Lamberti, C., DeBie, J. & Ferri, M. Respiratory signal derived from eight-lead ECG. In *Computers in Cardiology 1998*. 65–68 (IEEE, Cleveland, OH, USA, 1998). http://ieeexplore.ieee.org/document/731718/?arnumber=731718
41. Horowitz, M. & Meiri, U. Central and peripheral contributions to control of heart rate during heat acclimation. *Pflüg. Arch.* **422**, 386–392 (1993).
42. Hardy, J. D. Physiology of temperature regulation. *Physiol. Rev.* **41**, 521–606 (1961).